GENERAL PROBLEMS AND DIRECTIONS

Applications of Quantum Cloning[1]

E. Pomarico, B. Sanguinetti, P. Sekatski, H. Zbinden, and N. Gisin

Group of Applied Physics, University of Geneva, CH-1211 Geneva 4, Switzerland
e-mail: Bruno.Sanguinetti@unige.ch
Received April 18, 2011

Abstract—Quantum Cloning Machines (QCMs) allow for the copying of information, within the limits imposed by quantum mechanics. These devices are particularly interesting in the high–gain regime, i.e., when one input qubit generates a state of many output qubits. In this regime, they allow for the study of certain aspects of the quantum to classical transition. The understanding of these aspects is the root of the two recent applications that we will review in this paper: the first one is the Quantum Cloning Radiometer, a device which is able to produce an absolute measure of spectral radiance. This device exploits the fact that in the quantum regime information can be copied with only finite fidelity, whereas when a state becomes macroscopic, this fidelity gradually increases to 1. Measuring the fidelity of the cloning operation then allows to precisely determine the absolute spectral radiance of the input optical source. We will then discuss whether a Quantum Cloning Machine could be used to produce a state visible by the naked human eye, and the possibility of a Bell Experiment with humans playing the role of detectors.

INTRODUCTION

In the classical world information can be copied exactly, however the ability to do so in the quantum regime would lead to paradoxes such as Herbert's faster–than–light flash telegraph [1], which motivated Zurek and Wootters to develop the no cloning theorem [2], showing that quantum information cannot be copied perfectly. This concept is at the basis of quantum cryptography, as an eavesdropper attempting to duplicate information in a quantum communication channel will necessarily introduce errors and reveal his presence. So, if quantum information cannot be copied exactly, what is the best that can be done? This question can be answered by the theoretical and experimental study of Quantum Cloning Machines. In this article we will not examine quantum cloning as applied to cryptography, but rather review our recent work on how cloning can be used for two other purposes: first we demonstrate, both theoretically and experimentally, how quantum cloning can produce an absolute measure of spectral radiance [3]. In the second part of this article we examine whether a Bell–experiment could be made by amplifying (cloning) one photon, such that the measurement could be performed by a human's naked eye, and selecting the measurement basis just before the pupil. This thought experiment will help us to clarify certain important aspects of quantum mechanics such as what can be inferred by detecting a macroscopic (cloned) state and the importance of the detection loophole when performing a Bell inequality experiment. We will see that

what can be inferred about a cloned state strongly depends on the detection technology available [4]. Before looking at the individual applications, we will briefly describe the different types of cloning machine.

Cloning Machines

A cloning machine [5] will take a quantum state on its input, for example the polarisation of a photon, and produce multiple particles with a similar state on the output, so that if we measure the state of each output particle individually, on average it will have a fidelity $\mathcal{F}$ with respect to the input. If the measured $\mathcal{F}$ is equal to the theoretical maximum, the cloning machine is said to be optimal.

The process of stimulated emission is a good illustration of how cloning works: injecting a photon of a particular polarisation into a gain medium will produce more photons of the same polarisation. However, stimulated emission is always accompanied by spontaneous emission which will produce photons of random polarisation in the same spatiotemporal mode. As it is impossible to separate the photons emitted by the stimulated process from the ones emitted by the spontaneous process, noise will always be present at the output: this guarantees that the "no cloning" theorem is satisfied.

It is possible to optimise a cloning machine for a specific task. For example, if one has no a priori knowledge on the state to be cloned it is best to use a Universal Cloning Machine which will copy any arbitrary qubit with the same fidelity. However, if one has some knowledge of the input state, we can choose the

---

[1] The article is published in the original.

symmetry of the cloning process such that it clones more likely states with better fidelity at the expense of cloning more rare states with lower fidelity. One such device is the phase−covariant cloning machine, which is able to clone states on the equator of the Bloch sphere with increased fidelity at the expense of states lying outside of the equator. When high gains are desired (many output photons) a "measure and pre-pare" cloning machine will offer the same fidelity as a phase−covariant cloner, with the advantage of being less sensitive to losses before the cloning process and with the disadvantage of not being a unitary operation.

More formally, the universal cloner provides the following transformation:

$$a \rightarrow \sqrt{G}a + \sqrt{G-1}b^{\dagger}, \qquad (1)$$

where G is the gain parameter and b is the anti-clone mode (e.g., ions in a doped fiber). Its orthogonal mode $a_{\perp}$ obeys the same transformation where we replace b by $b_{\perp}$, and it is easy to see that this implies the same transformation for all photons on the Poincaré sphere. The anti-clone mode is initially empty in such a way that the photon number is transformed as

$$\langle 0_b | a^{\dagger}a | 0_b \rangle \rightarrow G a^{\dagger}a + (G-1). \qquad (2)$$

The phase covariant cloner may be achieved in the down-conversion scenario where the anti-clone mode b is matched with the clone mode a in such a way that

$$\begin{aligned} a &\rightarrow \sqrt{G}a + \sqrt{G-1}a^{\dagger}, \\ a_{\perp} &\rightarrow \sqrt{G}a_{\perp} + \sqrt{G-1}a_{\perp}^{\dagger}. \end{aligned} \qquad (3)$$

The photon number then obeys

$$a^{\dagger}a \rightarrow (2G-1)a^{\dagger}a + (G-1) + \sqrt{G(G-1)}(a^2 + a^{\dagger 2}), \quad (4)$$

which gives $a^{\dagger}a \rightarrow (2G-1)a^{\dagger}a + (G-1)$ for qubits (a^2 terms give zero), which give less noise and better fidel-ity than the universal cloner. It is easy to see that each mode that obeys $a_{\varphi} = \cos(\varphi)a + \sin(\varphi)a_{\perp}$ obeys the same transformation rule. However, if we go out of that circle on the Poincaré sphere this is to be modified. For the modes $a_h = (a + ia_{\perp})/\sqrt{2}$ and $a_v = (a - ia_{\perp})/\sqrt{2}$ the transformation is

$$\begin{aligned} a_h &= \sqrt{G}a_h + \sqrt{G-1}a_v^{\dagger}, \\ a_v &= \sqrt{G}a_v + \sqrt{G-1}a_h^{\dagger}. \end{aligned} \qquad (5)$$

The indices h and v are present because in real exper-iments these modes correspond to linear polariza-tions. This implies that the difference in number of photons between these two modes $a_v^{\dagger}a_v - a_h^{\dagger}a_h$ stays unchanged during cloning, so we create photons in pairs and the fidelity is very low for these modes. As its name indicates, the phase covariant cloning is only optimal for photons laying on the φ circle described above.

QUANTUM CLONING FOR AN ABSOLUTE RADIOMETRIC PRIMARY STANDARD

Background

Radiometry deals with the measurement of the properties of the electromagnetic radiation. Its incep-tion as a systematic and quantitative research field can be attributed to the first attempts in the 18th century to quantify the intensity of light produced by stars and the development of the theory of electromagnetism by Maxwell in 1864. Since then, one of the fundamental goal of radiometry has been the discovery of primary standards for the spectral radiance of optical sources.

The first radiometric approaches have exploited the equivalence between electromagnetic energy, heat and electrical energy. One of the first radiometers were based on the electrical substitution (ES) principle, according to which the heating effect of the optical radiation to be measured is compared with the heating effect produced via Joule effect by a measured electri-cal power. Measurements performed with these radi-ometers, such as the first observation by Lummer and Kurlbaum in 1892 [6] of the spectral distribution of the radiation emitted by a heated black body, led to the physical understanding by Planck in 1900 of the black body radiation spectrum based on quantum hypothe-sis. Historically, this has marked the beginning of a deep tie between radiometry and quantum mechanics. The ES radiometer is still used as the primary standard for spectral radiance by many metrology laboratories. The accuracy of these systems have been improved over more than a century and now uncertainties smaller than 0.01% can be achieved in cryogenic con-ditions [7]. ESRs show the highest accuracy when measurements of radiant flux are performed at the power level of hundreds of microwatts (10^{13} pho-tons/s).

Recently, the possibility of providing new primary standards by linear silicon photodetectors has been investigated. In this case photons do not produce heat by absorption but are converted directly into an elec-trical current, through the photoelectric effect. The deviation of the quantum efficiency from unity can be determined independently of other radiometric mea-surements, but uncertainties of this technique imple-mented with commercial photodiodes seem to be lim-ited. In any case, even if radiometric measurements find their explanation in quantum electrodynamics, the ES or the photodetector−based radiometers can-not distinguish the discrete nature of single photons. Nevertheless, quantum mechanics can offer concep-tually brand new primary standard methods in the sin-gle photon regime.

The quantum interpretation of non linear phenom-ena has offered in recent years another conceptually new primary standard method, which exploits the cor-relations in photon pairs produced by Spontaneous Parametric Down Conversion. The observation of one photon from a pair in a certain direction implies the
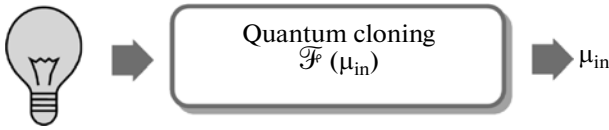
Fig. 1. Principle of the cloning radiometer.

presence of the other paired photon in the conjugated direction. This absolute technique is attractive because it relies simply on the counting of events, requires the measurement of few quantities and does not depend on any reference standard. This primary standard is particularly suited for the calibration of single photon detectors and the realization of absolute radiometric scales in the single photon regime [8, 9]. Therefore, this primary standard works for signal levels approaching picowatt and femtowatt (10^4–10^7 photons/s). The accuracy of this technique has been improved by nearly one order of magnitude every ten years reaching recently a relative uncertainty of 0.18% [10].

The Cloning Radiometer: Principle of Operation

In this paper we present another radiometric primary standard, which finds its basis in the quantum information theory. Classical information can be perfectly copied, independently of the initial quantity. This is not allowed in the quantum domain. Quantum information can be cloned only with a non unitary fidelity value. Moreover, this value depends on the quantity of information that needs to be cloned; in other terms the quality of the cloning changes for quantum systems with growing dimensions. In particular, Gisin and Massar in 1997 [11] proved that for an optimal quantum cloning machine (QCM), the fidelity of cloning N to $M > N$ identical qubits can be derived ab initio [11] to be

$$\mathcal{F}_{N \to M} = \frac{NM + N + M}{NM + 2M} = \frac{1 + 1/M + 1/N}{1 + 2/N}. \qquad (6)$$

The fidelity $\mathcal{F}_{N \to M}$ increases gradually to 1 for a growing number of input qubits N, that is the quality of the clones becomes perfect as the initial quantum information becomes classical. An absolute radiance measurement can be therefore realized by exploiting this particular aspect of the quantum to classical transition: by measuring the quality of the cloning one can estimate the number of input qubits.

The Eq. (6) remains valid for the cloning of polarization qubits distributed over a large number of modes and can be rewritten in terms of the average number of input and output photons per mode μ_{in} and μ_{out} [12]:

$$\mathcal{F}_{\mu_{in} \to \mu_{out}} \equiv \frac{\mu_{\parallel}}{\mu_{\parallel} + \mu_{\perp}} = \frac{\mu_{in}\mu_{out} + \mu_{in} + \mu_{out}}{\mu_{in}\mu_{out} + 2\mu_{out}}. \qquad (7)$$

μ_{out} can be expressed as the sum of the stimulated emission $G\mu_{in}$ and the spontaneous emission, equivalent to amplifying the vacuum, in such a way that

$$\mu_{out} = G\mu_{in} + 2(G - 1). \qquad (8)$$

Equations (7) and (8) can be combined to obtain the spectral radiance μ_{in} as a function of fidelity and gain:

$$\mu_{in} = \frac{2\mathcal{F}G - G - 2\mathcal{F} + 1}{G - \mathcal{F}G} \simeq \frac{2\mathcal{F} - 1}{1 - \mathcal{F}}, \qquad (9)$$

where we have written $\mathcal{F}$ in the place of $\mathcal{F}_{\mu_{in} \to \mu_{out}}$ for simplicity. The approximation in (9) holds for $G \gg 1$. From Eq. (9) it is evident that measuring the fidelity of the cloning process allows to directly estimate the number of input photons per mode μ_{in}, that is the input spectral radiance. The optical power of a light source under test at the input of the optimal QCM P_{in} can then be derived from μ_{in} by measuring the number of modes per unit time. The principle of the cloning radiometer is shown in Fig. 1.

What makes this method very interesting from a practical point of view is that the fidelity can be determined by a relative measurement. In the case of an optimal QCM of input polarization photonic qubits, the fidelity is given by the mean overlap between the input and output polarizations, and can be expressed as follows:

$$\mathcal{F} = P_{\parallel}/(P_{\parallel} + P_{\perp}), \qquad (10)$$

where $P_{\parallel}$ and $P_{\perp}$ are the output powers in the polarizations parallel and perpendicular to the polarization of the input light. Notice that the light at the input of the cloning machine must be in a pure state of polarization; if it is not, one measurement for each polarization must be made. Since the device measuring the fidelity does not need to be calibrated, this is an absolute primary standard method, based on a fundamental principle of quantum information.

Experimentally, optimal cloning has been implemented by stimulating parametric downconversion in bulk nonlinear crystals [13, 14]. Unfortunately, for reaching very high amplification gains, particularly powerful pump powers and system stability are needed [15]. Universal optimal quantum cloning can even be realized by stimulated emission in atomic systems [16, 17], as in Er^{3+} doped fiber amplifiers [12].

In this paper we propose a radiometer inspired by the above mentioned idea, which is based on a home-made Er^{3+} doped fiber amplifier. Three aspects make this scheme attractive: the first is that after amplification input power information is polarization encoded and is therefore insensitive to losses[2]; the second is

---

[2] The effect of Polarization Dependent Losses (PDL) is mitigated by averaging over a number of random polarizations produced by the scrambler.
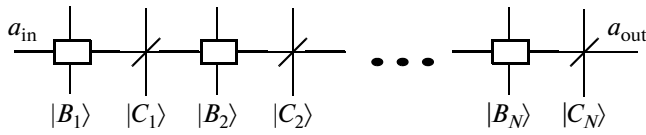
Fig. 2. Symbolical representation of the lossy amplification of mode a as a sequence of distinct amplifying elements (rectangles) spaced out by beam splitters (/ signs). $|B_n\rangle$ and $|C_n\rangle$ stand for the initial states of the local auxiliary modes.
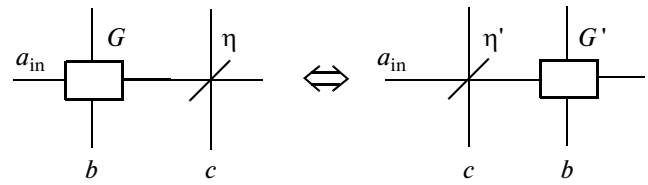

Fig. 3. The situations where the loss comes before or after the amplification are physically equivalent if the scalar parameters (G, η) and (G', η') satisfy (15).

that the experiment can be performed entirely in fiber, ensuring the selection of a single spatial mode. The third advantage is that this scheme works over a broad scale of powers: from single photon levels up to several tens of nW ($\sim 10^{11}$ photons/s).

Treatment of Losses

The reasoning presented above assumes the universal cloning process to be optimal. It has been shown theoretically that amplification in an inverted atomic medium indeed provides optimal cloning [16]. In order to evaluate the practical feasibility of optimal universal quantum cloning via stimulated emission in an Er^{3+} doped fiber, we should take into account the potential effects of internal losses. The amplification medium can be naively modeled, as shown in Fig. 2, as a sequence of thin amplifying atomic slices spaced out by beam splitters, representing the internal optical losses. The photonic propagation on the mode a in a lossy amplifier can be seen as successive interaction with these elements.

The action of the nth beam-splitter on modes a and c_n, an auxiliary mode initially in the vacuum state ($|C_n\rangle = |0\rangle_{c_n}$), can be expressed in the Heisenberg picture as

$$a^L = \sqrt{\eta_n} a + \sqrt{1 - \eta_n} c_n, \qquad (11)$$

where 'L' stands for losses and η_n is the specific transmission coefficient of the beam-splitter element.

A similar relation can be found for the amplifying element. By exploiting the equivalence between the amplification achievable by stimulated emission in an inverted atomic medium and by stimulated parametric down conversion in nonlinear crystals [17], the action of the amplifying element on modes a and b_n an auxiliary mode initially in the vacuum state ($|B_n\rangle = |0\rangle_{b_n}$), in the Heisenberg picture yields

$$a^A = \sqrt{G_n} a + \sqrt{(G_n - 1)} b_n^\dagger, \qquad (12)$$

where 'A' stands for amplification and G_n is the specific gain value of the nth amplifying element.

Let us consider now the two different situations represented schematically in Fig. 3. In the first case the propagation mode a_{in} passes through an amplifying element of gain G before interacting with mode c in a beam splitter of transmission η. In the second situation the order is inverted with the parameters G' and η'. Using Eqs. (11) and (12) the value of a at the output for the two cases is

$$a_{\text{out}}^1 = \sqrt{G\eta} a_{\text{in}} + \sqrt{\eta(G-1)} b^\dagger + \sqrt{1-\eta} c, \qquad (13)$$

$$a_{\text{out}}^2 = \sqrt{G'\eta'} a_{\text{in}} + \sqrt{(G'-1)} b^\dagger + \sqrt{G'(1-\eta')} c. \qquad (14)$$

Suppose that we fix the value of G and η and solve for the value of G' and η' that would give the same output $a_{\text{out}}^1 = a_{\text{out}}^2$. The system of equations that we get by these conditions always has the solution

$$\begin{cases} G' = \eta(G-1) + 1, \\ \eta' = G\eta/[G\eta + (1-\eta)]. \end{cases} \qquad (15)$$

The consequence of this result is that we can pull all the beam-splitter elements in Fig. 2 on the left, if we take care of correctly modifying the characteristic parameter for each element, obtaining the resulting transmission rate

$$Q = \prod_n \eta_n', \qquad (16)$$

with

$$\eta_n' = \frac{G_0^n \eta_n}{G_0^n \eta_n + (1 - \eta_n)} \approx 1 - \frac{1 - \eta_n}{G_0^n}, \qquad (17)$$

where $G_0^n = G_1 \ldots G_n$ is the effective gain between the beginning of the amplifier and element η_n. The approximation holds for small loss ($\eta_n \lesssim 1$).

The same is valid for the series of amplification layers giving a total amplification $\tilde{G} = \prod_n G_n'$. So the initial process represented in Fig. 2 can be equivalently seen as a transmission loss Q before an amplification $\tilde{G}$.

A fully inverted medium would have $Q = 1$. From Eq. (17) it is apparent that the effect of a small loss ($\eta_n \lesssim 1$) is proportional to $1/G_0^n$. As G_0^n grows exponentially over the length of the fiber, losses towards the end can be neglected. At the beginning of the amplifier two effects guarantee that the medium is fully inverted: the input signal is small, as it has not been amplified yet, and the signal and pump co-propagate, ensuring
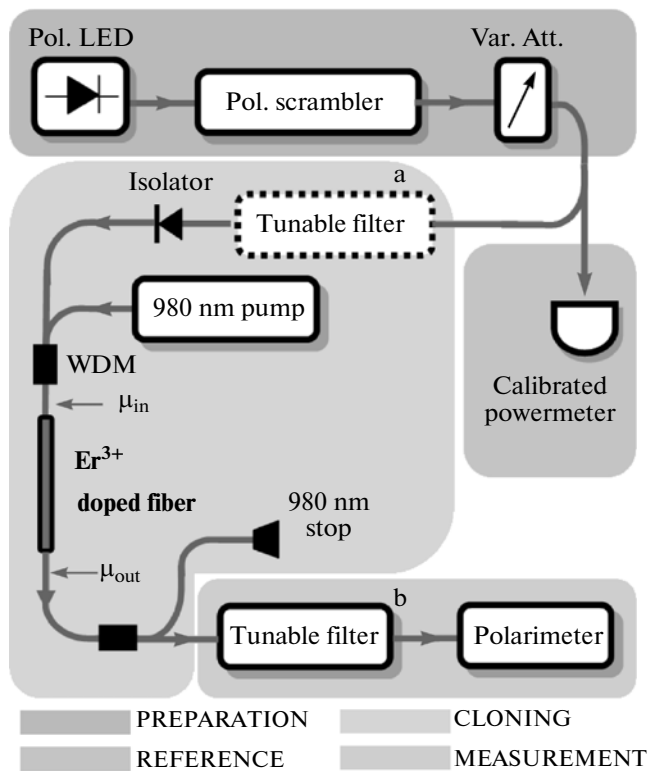
Fig. 4. Setup of the experiment.

Labels in figure:
Pol. LED — Pol. scrambler — Var. Att.
Isolator — Tunable filter — a
980 nm pump
WDM — μ_{in}
Er^{3+} doped fiber — 980 nm stop — μ_{out}
Tunable filter — b — Polarimeter
Calibrated powermeter

PREPARATION — CLONING
REFERENCE — MEASUREMENT

maximum pump power in this region. Cloning optimality can then be achieved in a non-ideal amplifier.

Experimental Setup

The setup of the experiment is shown in Fig. 4, It can be conceptually divided in four main parts: preparation of a set amount of power, comparison between the power measured by the cloning radiometer and that determined by a calibrated reference powermeter, realization of optimal cloning through the optical amplification by an Er^{3+} fiber and fidelity measurement.

To test our system, we prepare states with a known number of photons per mode (μ_{in}). This is done using a polarized LED at telecom wavelength that is passed through a polarization scrambler and a variable attenuator. The scrambler chooses a new random polarization before each experiment, which is repeated at a rate of 200 Hz.

The power is then split (50 : 50), with one branch monitored on a calibrated powermeter, while the other is sent to the amplification stage. The powermeter (EXFO PM−1100) has been recently calibrated by the Swiss national institute of standards (METAS) to an absolute uncertainty of 0.7% and with a measurement to measurement standard deviation of 0.5% (including fiber re-connection).

Optimal cloning is provided by 2 m of Er^{3+} doped fiber (attenuation 16.7 dB/m at 1530 nm), pumped by a 980 nm diode laser. The pump light is combined with the signal on the input of the Er^{3+} fiber using a wavelength division multiplexer (WDM), and an isolator is placed before the input to prevent unwanted resonances. After the Er^{3+} doped fiber, most of the pump power is removed using an additional WDM. In this realization, the no-cloning theorem is guaranteed by the Er^{3+} spontaneous emission, which adds randomly polarized photons to the signal.

The measurement stage consists of a grating-based tunable filter and a polarimeter (Profile PAT 9000). The filter has a width of 273.3(5) pm (FWHM). It serves two purposes: the first is to precisely determine the spectral width, and therefore the coherence time of the light, and the second is to ensure that polarization mode dispersion is negligible. The polarimeter measures the degree of polarization (DOP) with a nominal accuracy of 1%, where the DOP is defined as the polarized power (in any basis) P_{pol} over the total power P_{tot}, and is related to fidelity by $\mathcal{F} = (1 + \mathrm{DOP})/2$. Using a polarimeter rather than simply a polarizing beamsplitter and powermeter is less accurate, but allows us to test whether the system works equally well for arbitrary input states of polarization, i.e., whether the QCM is truly universal.

Experimental Procedure and Results

First of all we verify that the gain per unit length is constant over the entire Er^{3+} fiber, indicating that the atomic medium is fully inverted. We used an optical frequency−domain reflectometer [18], which measures the backscattering signal through the fiber and allows, in our case, to get information about the local amplification of the input light. Results are shown in Fig. 5. They show an exponential behaviour of the amplification, which is expected for a stimulated emission process.

To evaluate the accuracy of our system, we will need to compare our measurement of μ_{in} with the value μ_{in}^{*} obtained from the reference powermeter. We first measure the ratio between the power at the monitor output and the power at the entrance of the amplifier within the bandwidth of the tunable filter. This is done by placing the filter just before the amplification stage (position 'a' in Fig. 4). Together with a measurement of the filter's attenuation, this allows us to obtain the power at the input of the Er^{3+} doped fiber from the monitor powermeter P_{in}^{*}. The value of μ_{in}^{*} has to be derived from this value of power. Only the number of temporal modes per second need to be measured since we are using a single-mode fiber which ensures that there is only a single spatial mode. Therefore, we have to determine the frequency bandwidth of the filter or, equivalently, the coherence time of the filtered pho-
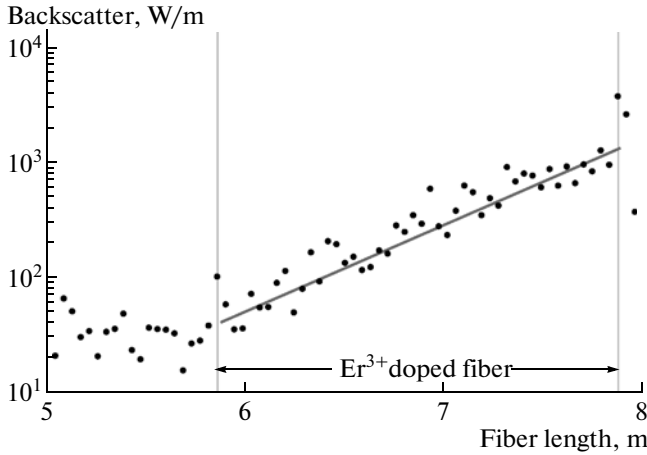
Fig. 5. Optical frequency—domain reflectometer measurement showing homogenous gain per unit length within the Er^{3+} doped fiber. The solid line is an exponential fit of the data.
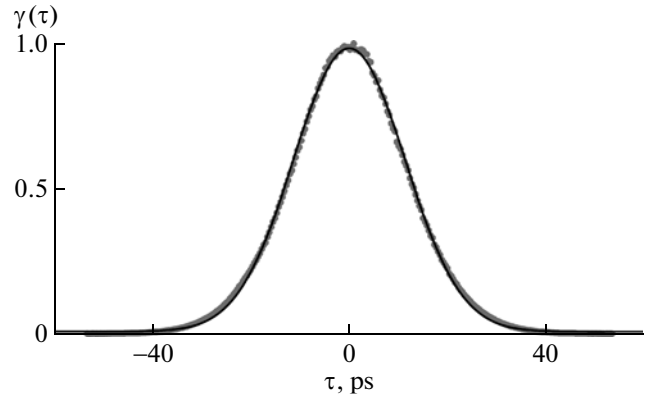

Fig. 6. Autocorrelation function of the source after the filter. $\gamma(\tau)$ is the fringe visibility measured with a low-coherence interferometer; τ_c will simply be the numerical integral of the square of this data. The solid line is a Gaussian fit.

tons. It is convenient to define the coherence time τ_c as in [19]:

$$\tau_c = \int_{-\infty}^{\infty} |\gamma(\tau)|^2 \, d\tau, \tag{18}$$

where $\gamma(\tau)$ is the autocorrelation function normalized such that $\gamma(0) = 1$. Using this definition, the coherence length $c\tau_c$ is the length of the unit cell of photon phase space [19], so that the number of modes per second is simply τ_c^{-1}. Measuring this value with an optical low-coherence interferometer (Fig. 6) yields, $\tau_c = 19.71(4)$ ps, which corresponds, assuming a Gaussian shape, to wavelength FWHM of $\Delta\lambda = 273.3(5)$ pm. We also performed a (less precise) spectrometric measurement yielding $\Delta\lambda = 271$ pm. With this filter, a mean of one photon per temporal mode corresponds to 6.461 nW.

μ_{in}^* can thus be estimated as the ratio between the number of input photons per unit time n_{in}^* (corresponding to P_{in}^* and the number of modes n_{modes}:

$$\mu_{in}^* = \frac{n_{in}^*}{n_{modes}} = \frac{P_{in}^* \tau_c}{E_{ph}} = \frac{P_{in}\lambda\tau_c}{hc}, \tag{19}$$

where E_{ph} is the energy of a single photon.

At this point we measure the amplifier gain of the Er^{3+} doped fiber to be $G = 66.5(3)$ by directly comparing the power at the output of the amplifier with the power at the input. The inset of Fig. 7 shows a typical plot, in terms of u_{in}^* and μ_{out}^*. μ_{out}^* is the number of photons per mode at the output of the Er^{3+} doped fiber: it is obtained from the value of power measured by the polarimeter's internal powermeter and calcu-

lated by considering the output losses (especially in the output WDM) and using the Eq. (19).

The thickness of the line in the inset of Fig. 7 represents random errors. Note from Eq. (8) that the gain is $G = \partial\mu_{out}/\partial\mu_{in}$; so that any systematic error in either the power measurement or the estimation of the number of modes cancels. The line in the inset of Fig. 7 is a fit of the data for $\mu_{in}^* < 1$, revealing that at high μ_{in} the gain is reduced. Pumping at the beginning of the Er^{3+} doped fiber allows the atoms to be inverted most likely at the beginning of the fiber. This effect could be minimized by pumping from both sides of the Er^{3+} doped fiber. Moreover, at high μ_{in}, so at the end of the fiber, the system is not sufficiently doped to amplify with the same gain a growing number of photons. Nevertheless, the gain is constant for $\mu_{in} < 2$, allowing us to assume within this range that the intercept μ_0 corresponds to the spontaneous emission $(2G - 2)$ from Eq. (8), so that: $\mu_{out} = G\mu_{in} + \mu_0$. In this range it is then possible to measure μ_{in} without distinguishing the polarizations, as $\mu_{in} = 2(\mu_{out}^* - \mu_{in}^*)/\mu_0^* - 2$.

We then measure the fidelity $\mathscr{F}$ versus μ_{in}^*: Fig. 7 shows a typical plot, which can be fitted with Eq. (9), where μ_{in} has been replaced with $k\mu_{in}^*$ and k is the fitted parameter. With this definition $k = \mu_{in}/\mu_{in}^*$ represents the discrepancy between our measurement of μ_{in} and the value μ_{in}^* obtained from the reference powermeter. Here, k also accounts for the possibility of non—optimal cloning which would introduce a further factor $Q \leq 1$, equivalent to a loss at the input of the cloning machine. The fitted curve in Fig. 7 yields $k = 1.013(5)$, where the indicated error represents statistical uncertainty. Systematic errors, as we shall see in the
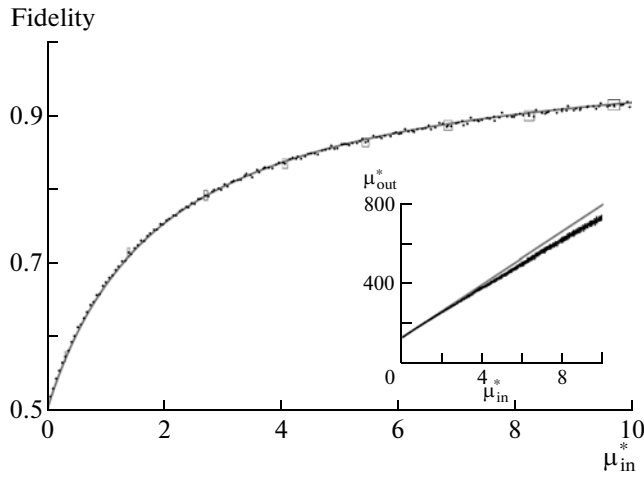
Fidelity

Fig. 7. Fidelity versus number of input photons per mode, fitted with Eq. (9). Representative errors are shown as boxes on some points. The inset shows the output versus input number of photons per mode, the line is a fit on the first data points ($\mu_{in}^* < 1$), showing reduced gain as μ_{in} grows.

next section, could be up to one order of magnitude higher.

Treatment of Errors

The aim of this experiment was to demonstrate the principle of a cloning radiometer, rather than to build a standard that can compete with metrology laboratories. It is however important to discuss the errors involved, both for the interpretation of the results and to evaluate the applicability of this method.

The primary standard that we have discussed in this paper consists in the estimation of a spectral radiance μ_{in} through a measurement of the cloning fidelity. The relationship between the fidelity and μ_{in} tells us how a small uncertainty in the fidelity $\Delta\mathscr{F}$ translates into an error in the measurement of μ_{in}. From Eq. (9) for $G \gg 1$ we obtain

$$\Delta\mu_{in} = \frac{\partial\mu_{in}}{\partial\mathscr{F}}\Delta\mathscr{F} = \frac{\Delta\mathscr{F}}{(1-\mathscr{F})^2}.$$

By expressing $\mathscr{F}$ as a function of μ_{in}, we find for high gains

$$\Delta\mu_{in} = (2+\mu_{in})^2\Delta\mathscr{F}.$$

$\Delta\mu_{in}/\mu_{in}$ has a minimum of $\Delta\mu_{in}/\mu_{in} = 8\Delta\mathscr{F}$ at $\mu_{in} = 2$, i.e., when spontaneous and stimulated emissions are equal. At higher spectral radiances, $\Delta\mu_{in}/\mu_{in}$ rises linearly with μ_{in}. The spectral bandwidth of the filter can be chosen as to operate in the desired power regime: our system is optimal at 13 nW, commercially available filters would allow this point to be easily lowered to 100 pW. From preliminary tests we estimate

that this technique would work to an upper limit of 100 nW, above which the effects of polarization mode dispersion and wavelength dependence of the components need to be taken into account.

There is also a series of systematic uncertainties that we have to take into account. One is due to the polarimeter. The polarimeter (Profile PAT 9000) is able to measure the degree of polarization (DOP) with a nominal uncertainty of $\Delta DOP = 10^{-2}$. We noticed that the fidelity was overestimated by 10^{-2} for unpolarized light, and underestimated by 2×10^{-3} for polarized light. Devices with a nominal accuracy of $\Delta DOP = 2.5 \times 10^{-3}$ and better are commercially available. The fidelity $\mathscr{F}$ is related to the DOP by $\mathscr{F} = (1+DOP)/2$, so that $\Delta\mathscr{F} = \Delta DOP/2 = 5\times 10^{-3}$. As discussed before, for $\mu_{in} = 2$, $\Delta\mu_{in}/\mu_{in} = 8\Delta\mathscr{F}$, so that the uncertainty contribution of the polarimeter is $\Delta\mu_{in}/\mu_{in} = 4\%$. In this experiment we used a commercial polarimeter for practical reasons, however the precision of this device is far from any fundamental limit: a polarimeter performs only a relative measurement of different polarization components which can be done very precisely. The precision of this relative measurement can then be transferred to the absolute measurement of spectral radiance via the cloning radiometer. The equations in the above paragraph show that the absolute measurement uncertainty will be only 4 times larger than the relative uncertainty. The uncertainties due to filter attenuation and insertion loss arise from the fact that the components' fibers are manually reconnected after the measurement. During this procedure, variations in the connector losses can occur on a level of 0.5%. The amplifier gain G can be determined precisely (0.5%), furthermore Eq. (9) in the article shows that a small variation $\Delta G/G$ will only affect $\Delta\mu_{in}/\mu_{in}$ by $\Delta G/G^2$ so that its effect on the measurement uncertainty is negligible at high gains. The above uncertainties affect our measurement of spectral radiance, however in the article we demonstrate the accuracy of our radiometer by relating the measured radiance to optical power and comparing our results with those obtained via a calibrated powermeter. In measuring k (the discrepancy between these two measurements) two further uncertainties come into play: the calibrated powermeter's absolute accuracy (0.7%) and the uncertainty in our measurement of coherence time (0.2%). A summary of the experimental uncertainties is shown in Table 1. A further complication arises from the Polarization Dependent Losses (PDL) of the various components. This effect is usually small ($\simeq 1\%$) and can therefore be eliminated by repeating the experiment for many different states of polarizations and averaging. The polarization scrambler is used for this purpose, by averaging over 20 different polarizations the mean PDL is reduced to below 0.2%. Table 2 summarizes the contribution of the various components to the PDL.

We would like to note that limits to the accuracy of the experiment do not arise from the principle of operation or from the cloning machine itself, but rather from the usual complications encountered when building a primary standard.

In conclusion we have demonstrated the theoretical principle and experimental feasibility of a radiometric primary standard based on optimal quantum cloning: by measuring the cloning fidelity one can directly determine the spectral radiance of an optical source. The system we develop is completely fiber–based and works in a broad range of optical powers at telecommunication wavelength. Our experimental realization of this standard shows an uncertainty on the spectral radiance of 1.3%, when compared with a calibrated powermeter, and 4%, when the error is calculated using the equipment's nominal uncertainties. However, it leaves a large margin for improvement by a metrology laboratory. Our experiment also shows that by Er^{3+} doped fiber amplification, optimal cloning of one to many qubits can be easily realized in spite of losses.

QUANTUM CLONING FOR A BELL EXPERIMENT WITH HUMAN EYES

Some predictions of quantum physics are so fascinating and counterintuitive that, since the birth of quantum mechanics, physicists try to find trace of its manifestation in the macroscopic world. In this perspective quantum cloning is very appealing, it appears as a natural candidate for bringing quantumness to macroscopic level. For example one can think of cloning an entangled pair of photons, which has been brilliantly done in Rome by the De Martini group using the phase covariant cloner [15]. States produced in this manner can contain a huge number of photons and can still be formally equivalent to an entangled photon pair (as in the case of lossless phase covariant cloning).

Experimental Setup

First, an entangled photon pair is produced in a low probability parametric down–conversion process and can be set to be in the singlet state

$$\left|\psi^{-}\right\rangle = (a_{\varphi}^{\dagger}b_{\varphi\perp}^{\dagger} - a_{\varphi\perp}^{\dagger}b_{\varphi}^{\dagger})\left|0\right\rangle / \sqrt{2}, \qquad (20)$$

with $\{\varphi, \varphi_{\perp}\}$ defining a basis on the Poincaré sphere. Then one of the photons, say the one in mode a, is amplified with different cloning machines. The detection of the other photon in mode b is used to trigger a successful creation of the pair.

Table 1. Contributions of the various components to the uncertainty of $\Delta\mu_{in}/\mu_{in}$. Values marked with an asterisk (*) only contribute to our measurement of k, i.e., the discrepancy of a power measurement performed with our apparatus with respect to one performed with a calibrated powermeter

Sources of error	Uncertainty, %
Polarimeter	4
Filter attenuation	0.5
Insertion loss	0.5
Gain	0.007
PDL	0.8
Powermeter	0.7
Coherence time*	0.2*
Total	4.1

Table 2. Summary of PDL of the different elements of the experiment

Sources of PDL	PDL, %
Filter	1.0
Attenuator	1.4
Powermeter	1.6
Isolator	<1.2
WDM	<2.0

Inferring Micro–Micro Entanglement with Human Eyes As Detectors

The frontier between the microscopic and the macroscopic world is not an objective ontological entity, for example one can argue that the cloned state contains tens of thousands of photons and is thus clearly macroscopic, but it can be retorted that the energy contained in such state is still of microscopic scale. One way of setting this frontier in our case is to ask the photonic state under consideration to be directly accessible to our senses, i.e., use human eyes as detectors.

The Human Eye

The human eye happens to be quite an efficient detector. If adapted to darkness, a person can see a light pulse of around ten photons. However, the probability that such a weak pulse is detected is small. This probability grows with the number of photons and attains one for few hundred photon pulses, depending on the person. The experimental behaviour for the human eye can be reproduced with a simple model [20]: an ideal threshold detector with efficiency limited by an imperfect transmission $\eta \approx 0.07$. In the Fock state representation the probability to have a
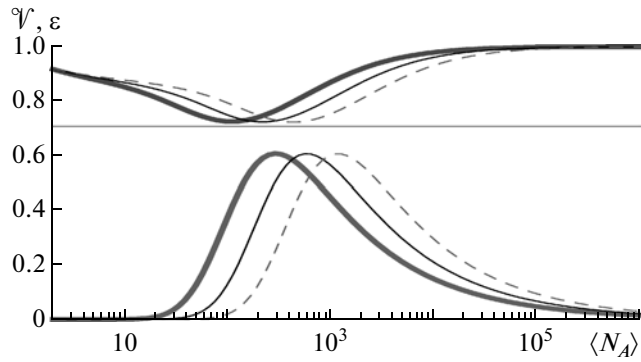
Fig. 8. Visibility of correlations $\mathcal{V}$ (upper curves) and the probability that a measurement is conclusive ε (lower curves) for the phase covariant cloner in function of the total number of photons in the amplified state. The dashed and the thin line show how this parameters change if we add losses after the amplification.

"click" with an ideal threshold detector is associated to the projector

$$\hat{T}_s(a) = 1 - \sum_{n \geq \theta} |n\rangle\langle n|, \qquad (21)$$

which gives 1 for Fock states with the number of photons exceeding the threshold θ (the threshold is around 7 for the human eye), and 0 in the other case. In Eq. (21) a denotes the measured mode that corresponds to $|n\rangle$. The imperfect transmission is modeled by a beam splitter U_{BS} acting on the ideal threshold operator

$$\hat{E}_s(a) = \langle 0_c | U_{BS}^\dagger \hat{T}_s(a) U_{BS} | 0_c \rangle. \qquad (22)$$

The action of the beam splitter is

$$U_{BS}^\dagger a U_{BS} = \sqrt{\eta}\, a + \sqrt{1-\eta}\, c,$$

where c is an initially empty auxiliary mode which is traced out.

The detection of the amplified side of the qubit is done in the following way. First a measurement basis $\{\varphi, \varphi_\perp\}$ is chosen by applying a linear optical element corresponding to the rotation of the Poincaré sphere that brings $\{\varphi, \varphi_\perp\}$ on $\{h, v\}$. The two linear polarizations (that now correspond to $\{\varphi, \varphi_\perp\}$) are separated on a PBS and then sent in two different detectors, which are human eyes in our case.

This measurement scenario has four possible outcomes, but the two cases where both eyes see or both do not see are considered inconclusive and are disregarded in further data analysis. The fact that we post-select only a part of all measurement events opens the detection loophole and we will return to this crucial point later. The other two events will be denoted P_φ

and $P_\varphi^\perp$ depending on which eye have seen the signal. The corresponding operators are

$$\hat{P}_\varphi = \hat{E}_s(a_\varphi) \otimes \left[1 - \hat{E}_s(a_{\varphi\perp})\right],$$
$$\hat{P}_\varphi^\perp = \left[1 - \hat{E}_s(a_\varphi)\right] \otimes \hat{E}_s(a_{\varphi\perp}). \qquad (23)$$

Note that for each cloner we only chose measurement basis among those that leave the state invariant.

Micro−Micro Entanglement

The detection scheme with human eyes described above can be used to design a CHSH violation experiment between the photon b and the amplified state. On the single photon side we take the binary observable $\mathcal{B}(\theta) = |1_\theta\rangle\langle 1_\theta| - |1_{\theta\perp}\rangle\langle 1_{\theta\perp}|$, while the observable on the amplified state is $\mathcal{A}(\varphi) = P_\varphi - P_\varphi^\perp$ that can have a value of -1 or 1. The value of the CHSH parameter after the post-selection is then given by the observable

$$\mathcal{S} = (1/\varepsilon)(\mathcal{A}(\varphi) \otimes \mathcal{B}(\theta) + \mathcal{A}(\varphi') \otimes \mathcal{B}(\theta) + \mathcal{A}(\varphi) \otimes \mathcal{B}(\theta') - \mathcal{A}(\varphi') \otimes \mathcal{B}(\theta')), \qquad (24)$$

where ε is the total probability of a conclusive detection given by the mean value $\langle P_\varphi + P_\varphi^\perp \rangle$. As in the single−photon case, $\mathcal{S}$ can be shown to vary with $\cos 2(\varphi - \theta)$, and for optimal settings the violation of CHSH is given by

$$\mathcal{S} = 2\sqrt{2}\mathcal{V}. \qquad (25)$$

$\mathcal{V}$ is the correlation visibility and is given by

$$\mathcal{V} = \langle P_\varphi - P_\varphi^\perp \rangle / \langle P_\varphi + P_\varphi^\perp \rangle, \qquad (26)$$

where the mean value is taken on the amplified $|1_\varphi\rangle$ state. From (25) we see that the local bound is violated if the visibility is higher than $1/\sqrt{2}$. The values of the visibility for the phase covariant cloner is reported in the Fig. 8. It can be shown that the universal cloner also allows to achieve visibilities higher than $1/\sqrt{2}$.

The Measure & Prepare Cloner and the Detection Loophole

Because of the results of the last section one is tempted to admit that there is indeed some non-locality between the single photon and the amplified state. However that is where the detection loophole comes into play. The fact that we disregard some of the measurement outcomes allows a whole new family of local models where the detector can choose to click or not depending on the measurement settings.

From this perspective it is not surprising that the measure & prepare cloner, that produces a separable state, also gives a violation of the CHSH inequality after post−selection [4]. This is a very nice illustration

of the importance of the detection loophole, that is sometimes considered as esoteric.

The conclusion may appear disappointing: if even a separable state passes our post−selective CHSH test, the test seems to teach us nothing about the states under consideration. However there is still something that can be done. Indeed it can be shown that for any cloner if the observed visibility $\mathcal{V}$ is above 1/2 then the photon pair before the clones was entangled. See [4] for more details.

Entanglement Witness and Micro−Macro Entanglement

Since the human eye Bell test doesn't give us knowledge about the entanglement of the single photon and the amplified state, we have to develop new tools that allow us to investigate this entanglement.

Following [21], we introduce a quantity that witnesses the entanglement between subsystems A and B. It has the following form:

$$W = |\langle \mathbf{J}_A \mathbf{J}_B \rangle| - \langle N_A N_B \rangle, \tag{27}$$

where $\mathbf{J}_A$ and $\mathbf{J}_B$ denote Stokes vectors (total polarization) on parts A and B, while N_A and N_B are the total number of photons for A and B. For any separable state $\sum_i p_i \rho_i \otimes \sigma_i$ we can bound $|\langle \mathbf{J}_A \mathbf{J}_B \rangle|$:

$$|\langle J_A J_B \rangle| \leq \sum_i p_i |\langle \mathbf{J} \rangle_{\rho_i} \langle \mathbf{J} \rangle_{\sigma_i}|$$

$$= \sum_i p_i |\langle J_z \rangle_{\rho_i'} \langle J_z \rangle_{\sigma_i'}| \leq \langle N_A N_B \rangle,$$

where the ' sign on the states ρ_i and σ_i means that we choose the basis where only the z component of $\langle \mathbf{J} \rangle_{\rho_i'}$ nonzero. Hence, the positivity of W means that A and B are entangled. In terms of photon number operators the Stokes vectors are $J_i = a_i^\dagger a_i - a_{i\perp}^\dagger a_{i\perp}$ on the amplified side and $J_i = |1_i\rangle\langle 1_i| - |1_{i\perp}\rangle\langle 1_{i\perp}|$ on the single photon side, with i denoting a particular basis. To evaluate W for the amplified singlet state, since the photon in mode b not amplified, we can directly take the mean value on it, and obtain

$$W = \sum_i \left(\langle a_i^\dagger a_i \rangle_1 - \langle a_i^\dagger a_i \rangle_0 \right) - \langle a_k^\dagger a_k \rangle_1 - \langle a_k^\dagger a_k \rangle_0. \tag{28}$$

Here $\langle \ \rangle_1$ is the mean value on the amplified $|1\rangle$ and $\langle \ \rangle_0$ is the mean value on the vacuum. Using the transformations of the photon number operator derived before we can easily find that the violation is $W = 2$ both for the universal and the phase covariant cloners. The losses after the amplification transform the photon number operator $a^\dagger a \to \eta a^\dagger a$ and the witness violation gets simply multiplied by the transmission $W = 2\eta$. And the entanglement is never completely broken. For the treatment of losses during and before the amplification and the persistence of entanglement the interested reader can look in [4].

In conclusion, we have shown that although it is possible to violate a Bell inequality using a cloned state and lossy threshold detectors, such as human eyes, this can only be done with limited efficiency, by opening up the detection efficiency loophole.

REFERENCES

1. N. Herbert, Found. Phys. **12**, 1171 (1982).
2. W. K. Wootters and W. H. Zuker, Nature **299**, 802 (1982).
3. B. Sanguinetti, E. Pomarico, P. Serkatski, H. Zbinden, and N. Gisin, Phys. Rev. Lett. **105**, 080503 (2010).
4. P. Sekatski, B. Sanguinetti, E. Pomarico, N.Gisin, and C. Simon, arXiv quant-ph 1005.5083v1 (2010).
5. V. Scarani, S. Iblisdir, N. Gisin, and A. Acin, Rev. Mod. Phys. **77**, 1225 (2005).
6. O. Lummer and F. Kurlbaum, Ann. Phys. **282**, 204 (1892).
7. J. Zwinkels, E. Ikonen, N. Fox, G. Ulm, and M. Rastelli, Metrologia (2010).
8. D. C. Burnham and D. L. Weinberg, Phys. Rev. Lett. **25**, 84 (1970).
9. S. V. Polyakov and A. L. Migdall, Opt. Express **15**, 1390 (2007).
10. S. V. Polyakov and A. L. Migdall, J. Mod. Opt. **56**, 1045 (2009).
11. N. Gisin and S. Massar, Phys. Rev. Lett. **79**, 2153 (1997).
12. S. Fasel, N. Gisin, G. Ribordy, V. Scarani, and H. Zbinden, Phys. Rev. Lett. **89**, 107901 (2002).
13. F. D. Martini, Opt. Commun. **179**, 581 (2000).
14. A. Lamas-Linares, C. Simon, J. C. Howell, and D. Bouwmeester, Science **296**, 712 (2002).
15. F. D. Martini, F. Sciarrino, and C. Vitelli, Phys. Rev. Lett. **100**, 253601 (2008).
16. C. Simon, G. Weihs, and A. Zeilinger, Phys. Rev. Lett. **84**, 2993 (2000).
17. J. Kempe, C. Simon, and G. Weihs, Phys. Rev. A **62**, (2000).
18. M. Wegmuller, P. Oberson, O. Guinnard, C. Vinegoni, and N. Gisin, J. Lightwave Technol. **18**, 2127 (2000).
19. L. Mandel and E. Wolf, Proc. Phys. Soc. **80**, 894 (1962).
20. H. Barlow, J. Opt. Soc. Am. **46**, 634 (1956).
21. P. Sekatski, N. Brunner, C. Branciard, N. Gisin, and C. Simon, Phys. Rev. Lett. **103**, 113601 (2009).